Interactions between Cytochrome c_2 and Photosynthetic Reaction Center from *Rhodobacter sphaeroides*: Changes in Binding Affinity and Electron Transfer Rate Due to Mutation of Interfacial Hydrophobic Residues Are Strongly Correlated[†]

Xiao-Min Gong, Mark L. Paddock, and Melvin Y. Okamura*

Department of Physics 0319, 9500 Gilman Drive, University of California San Diego, La Jolla, California 92093-0319

Received September 5, 2003; Revised Manuscript Received October 16, 2003

ABSTRACT: The structure of the complex between cytochrome c_2 (cyt) and the photosynthetic reaction center (RC) from *Rhodobacter sphaeroides* shows contacts between hydrophobic residues Tyr L162, Leu M191, and Val M192 on the RC and the surface of the cyt [Axelrod et al. (2002) *J. Mol. Biol. 319*, 501−515]. The role of these hydrophobic residues in binding and electron transfer was investigated by replacing them with Ala and other residues. Mutations of the hydrophobic residues generally resulted in relatively small changes in the second-order electron-transfer rate k_2 (Brönsted coefficient, $\alpha = 0.15 \pm 0.05$) indicating that the transition state for association occurs before short-range hydrophobic contacts are established. Larger changes in k_2, found in some cases, were attributed to a change in the second-order mechanism from a diffusion controlled regime to a rapidly reversible binding regime. The association constant, K_A, of the cyt and the rate of electron transfer from the bound cyt, k_e, were both decreased by mutation. Replacement of Tyr L162, Leu M191, or Val M192 by Ala decreased K_A and k_e by factors of 130, 10, 0.6, and 120, 9, 0.6, respectively. The largest changes were obtained by mutation of Tyr L162, showing that this residue plays a key role in both binding and electron transfer. The binding affinity, K_A, and electron-transfer rate, k_e were strongly correlated, showing that changes of hydrophobic residues affect both binding and electron transfer. This correlation suggests that changes in distance across hydrophobic interprotein contacts have similar effects on both electron tunneling and binding interactions.

Interprotein electron-transfer reactions are important for energy conversion in photosynthesis and respiration (*1*, *2*). The dynamics of this process involves the docking of two proteins, positioning the electron donor and acceptor cofactors into the proper configuration for electron transfer (*3*), followed by electron transfer in the active complex (*4*). The structure and interactions of the two proteins at the interface are important in determining the rates of electron transfer. Long-range electrostatic interactions play an important role in the docking and hence influence the association process (*2*, *3*, *5*, *6*). However, the role of hydrophobic interactions in these processes is less well understood. Recently, the X-ray crystal structure of the complex between the electron-transfer proteins cytochrome c_2 (cyt)[1] and the reaction center (RC) from the photosynthetic bacterium *Rhodobacter sphaeroides* was determined, and contacts between hydrophobic residues were observed (*7*). In this work, we have examined the effects of modifying hydrophobic residues on the RC on the binding and intermolecular electron-transfer reaction between the two proteins.

The RC is a membrane protein that is involved in the initial light-induced electron-transfer reactions in bacterial photosynthesis (*8*). Light absorbed by the RC initiates an intramolecular electron-transfer reaction oxidizing a primary electron donor, a bacteriochlorophyll dimer D, and reducing a quinone acceptor Q_B. The oxidized donor D^+ is reduced by a water-soluble electron carrier protein, cytochrome c_2, that is part of a chain of electron carriers including the cytochrome bc1 complex. This system cycles electrons through the RC and pumps protons across the membrane (*9*).

The reaction between cyt and RC in detergent solutions has been extensively studied (*10*−*14*). See ref *15* for a review. A two-state model that accounts for the observations is shown below.

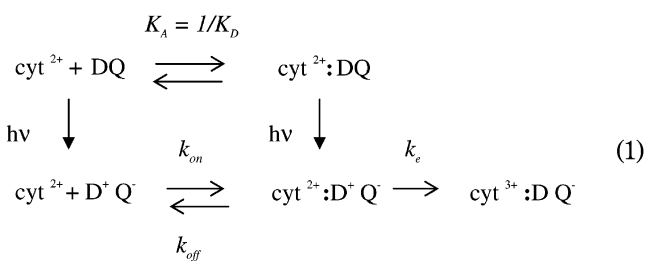

(1)

where K_A is the association constant and K_D is the dissociation constant, k_{on} is the second-order rate constant for binding, k_{off} is the dissociation rate constant, and k_e is the first-order electron-transfer rate constant ($k_e = 1/\tau_e$). DQ represents the

[†] This work was funded by grants from NSF MCB99-74568 and NIH GM41637.

* To whom correspondence should be addressed: Phone: 858-534-2505 Fax: 858-822-0007, E-mail: mokamura@ucsd.edu.

[1] Abbreviations RC, reaction center; cyt, cytochrome; D, bacteriochlorophyll dimer (donor); Q, quinone; α, Brönsted coefficient; β, distance decay parameter.

10.1021/bi035603c CCC: $25.00
Published on Web 11/20/2003

RC, and cyt/DQ represents the docked complex. Reduced cyt and RC in solution are in equilibrium with a bound cyt/RC complex with a dissociation constant $K_D \sim 10^{-6}$ M at low ionic strength, shown on the top line in eq 1. Excitation of the RC by a laser flash forms the charge-separated state D^+Q^-. In the presence of cyt c_2 re-reduction of D^+ occurs in two phases. The cyt bound on the RC is rapidly oxidized in a fast phase ($k_e \sim 10^6$ s^{-1}) (*15*), while the free cyt reacts via a second-order reaction in a slow reaction with a second-order rate constant $k_2 \sim k_{on} \sim 10^9$ s^{-1} M^{-1} (ionic strength ~ 10 mM) (*15*) and dissociation rate constant $k_{off} \sim 10^3$ s^{-1} (*17*).

The role of electrostatic interactions on the binding and electron-transfer reactions between cyt and RC were shown by the dependence of the second-order rate constant and dissociation constant on ionic strength (*10*). The importance of charged side chains was demonstrated by chemical modification (*18*), chemical cross-linking (*19*), and site-directed mutagenesis (*14*, *20*, *21*). The periplasmic surface of the RC contains regions of negatively charged residues, while the surface of the cyt near the exposed heme edge contains regions of positively charged residues. Several models of the cyt/RC complex have been proposed based on the juxtaposition of surface charges to form salt bridged ion pairs (*22*−*24*). More recently, Tiede et al. (*25*) proposed that the electrostatic interactions in the cyt/RC complex are due to the overlap regions of positive and negative potential rather than specific ion pair interactions. Their conclusion was based on the observation that tight binding of cyt from different species having different distributions of charged residues on the binding surface and on electrostatic calculation of the surface potentials of cyt and RC. Electrostatic calculations based on the cocrystal structure show that while long-range electrostatic interactions are important for docking they do not determine the structure of the bound state (*6*).

The involvement of hydrophobic interactions on the electron-transfer reaction was shown by mutations of Tyr L162 on the RC from *Rb. sphaeroides* (*26*, *27*) that greatly decreased the measured rate of electron transfer with cyt. Since mutations of Tyr L162 in *Rhodopseudomonas viridis*, where the cyt is permanently bound to the RC, did not produce significant changes in electron-transfer rate (*28*), the changes in rate observed in *Rb. sphaeroides* RCs are most likely due to changes in the position of the cyt bound to the RC surface due to replacement of Tyr L162. Tetreault et al. (*14*) proposed a two-domain model that incorporates both electrostatic and short-range hydrophobic interactions to explain why mutating charged interface residues had large effects on K_D and k_2 but small effects on k_e. In this model, long-range electrostatic interactions due to charged residues stabilize the cyt/RC complex and are important for docking. But short-range interactions due to uncharged surface residues guide the juxtaposition of the heme group of the cyt on the RC surface for fast electron transfer.

The X-ray crystal structure of the *Rb. sphaeroides* cyt/RC complex provides information about electrostatic and hydrophobic interactions (*7*). Positively charged residues from the cyt are positioned opposite to negatively charged residues across the cyt RC interface. In addition, short-range contacts between hydrophobic patches on cyt and RC are observed. Several key hydrophobic residues are shown in Figure 1. The exposed heme edge of the cyt is in van der Waals contact with Tyr L162, located directly above $BChl_2$. In addition, van der Waals contacts are found between two hydrophobic residues Leu M191 and Val M192 on the RC and the heme edge and a hydrophobic residue Phe C102 on the cyt (Figure 1). The structure suggests that these hydrophobic residues may be important for binding and electron transfer. A preliminary account of this work has been presented (*29*).

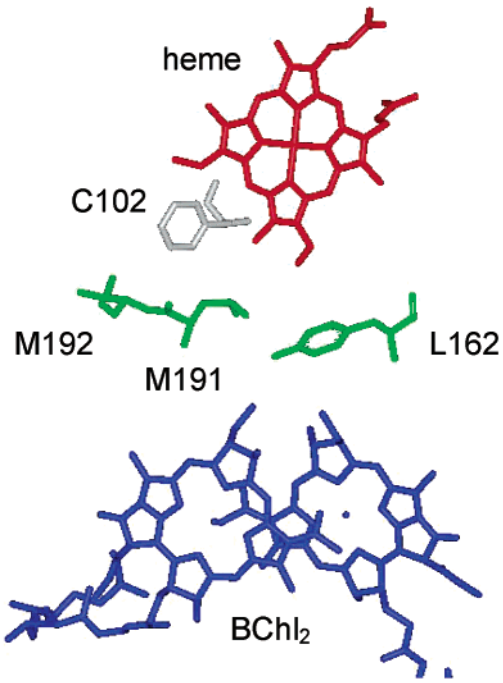

FIGURE 1: Structure of cofactors and hydrophobic residues at the interface of the cyt/RC complex. The electron-transfer cofactors heme (red) and BChl2 (blue) are shown with hydrophobic residues Tyr L162 (green), Leu M191 (green), and Val M192 (green) on the RC and Phe C102 (gray) on the cyt.

In the present work, the role of the hydrophobic residues in binding and electron transfer were examined to test the validity of this suggestion. RC mutants were constructed in which the hydrophobic residues Tyr L162, Leu M191, and Val M192 were changed to other residues to examine the effects of these mutations on the binding and electron-transfer reaction. The results show changes in the binding and first-order and second-order electron-transfer rates. An interesting correlation between binding and first-order electron-transfer rate is observed. The results provide information about the nature of hydrophobic interactions and their role in binding and electron transfer.

MATERIALS AND METHODS

Samples. The Tyr L162 mutants modified to Phe, Leu, and Ser were constructed as described previously (*26*). The remaining RC mutants were constructed using the thermocycling method described in ref *30*. The cells harboring the mutant RCs were grown and isolated as previously described (*31*). RCs were expressed in the deletion strain of *Rb. sphaeroides*, ΔLM1, which was grown aerobically to avoid selection of revertants. The RC concentration was determined from the optical absorbance at 802 nm, using $\epsilon^{RC}_{802nm} = 288$ mM^{-1}cm^{-1}. Protein purity was characterized by the optical absorbance ratio: A_{280}/A_{802}. This ratio was always less than 1.50, and in most samples it was less than 1.30. Cytochrome

c_2 was isolated as described (*32*) from a photosynthetically grown cyt c_2 overproducing strain of *Rb. sphaeroides*, cycA1-containing copies of the plasmid pC2 P404.1 (*33*). The cyt c_2 concentrations were determined from their optical absorbancies at 550 nm, using $\epsilon_{550\ nm}$ (reduced) = 30.8 mM^{-1} cm^{-1} (*32*). Protein purity was characterized by the optical absorbency ratio: A_{280}/A_{417}, which was ≤ 0.25.

Electron-Transfer Measurements. The kinetic measurements were made as described (*14*) using transient absorption spectroscopy. The reactions were initiated by a laser pulse from a Nd:YAG laser equipped with a tunable optical parametric oscillator (Opotek, λ = 800 nm, τ = 10 ns). Absorption changes accompanying electron transfer were monitored at either 595 or 865 nm using a modified Cary 14 spectrophotometer (Varian). Flash-induced absorbance data were collected on a Le Croy oscilloscope and transferred to a computer for analysis. All measurements were performed at 23 °C in a buffer of 10mM Hepes, 0.04% β-D-maltoside, and 0.1 mM EDTA at pH 7.5. Prior to measurements of binding and second-order kinetics, 40 μM each of Q_0 and Q_0H_2 were added as a redox buffer, ensuring that cyt c_2 was fully reduced before each laser flash. For measurements of first-order kinetics, higher concentrations (200 μM) of Q_0 and Q_0H_2 were used to maintain the cytochrome in the fully reduced state.

The binding affinity and second-order rate constants were determined by monitoring the absorbance changes due to oxidation of D to D^+ at 865 nm on samples having a RC concentration of ~0.2 μM. Lower concentrations (0.1 μM) were used for RCs having tighter binding to allow accurate determination of the free cyt concentration [cyt^{2+}]. For samples displaying biphasic kinetics the dissociation constant K_D was determined by monitoring the absorbance changes of the fast and slow phases ΔA_f and ΔA_s fit to the relation

$$\Delta A = \Delta A_f\, e^{-k_e t} + \Delta A_s e^{-k_s t} \tag{2}$$

where k_e is the fast rate constant associated with electron transfer from the bound cyt in the complex and k_s is the rate constant for the slow phase of electron transfer due to the association of the free cyt with the RC. The values of K_D were obtained from the fraction of bound cyt determined from the dependence of the amplitudes of the fast and slow phases on the concentration of free cyt.

$$\text{fraction bound} = \frac{\Delta A_f}{\Delta A_f + \Delta A_S} = \frac{1}{1 + \dfrac{K_D}{[cyt^{2+}]}} \tag{3}$$

The change in free energy $\delta\Delta G$ due to mutation of a residue is calculated by

$$\delta\Delta G = k_B T \ln\left(\frac{K_D(\text{mutant})}{K_D(\text{native})}\right) \tag{4}$$

where k_B is Boltzmann's constant and T is the absolute temperature. The second-order rate constant, k_2, was determined from the observed rate of the slow phase of the electron transfer, k_S, under conditions where the concentration of free cyt c_2, [cyt^{2+}] was large compared to the unbound RC concentration, [RC^+] so that the reaction, d[RC^+]/dt = k_2[cyt^{2+}][RC^+], is pseudo first-order. The pseudo first-order rate constant,

$$k_s = k_2[cyt^{2+}] \tag{5}$$

was plotted versus free cyt c_2 concentration to obtain the second-order rate constant. For some RCs exhibiting tight cyt binding, and thus low concentrations of free cyt, the rates were measured at higher ionic strength and the rate constants were extrapolated to lower ionic strength. The first-order rate constant, k_e, was measured at a higher RC concentration of ~5 μM. The re-reduction of the donor was monitored at 595 nm to avoid flash artifacts from laser excitation.

In some mutant RC samples, monophasic decay kinetics were observed at all cyt concentrations. The observed rate constant, k_{obs}, increased with increasing cyt concentration to a saturating value, k_e, following the Michaelis Menton relation. In these cases, the K_D and k_e were obtained by fitting the observed concentration dependent rate constant k_{obs}, to the steady-state equation.

$$k_{obs} = \frac{k_e}{1 + \dfrac{K_M}{[cyt]}} \tag{6}$$

where

$$K_M = \frac{k_{off} + k_e}{k_{on}} = K_D + \frac{k_e}{k_{on}} \tag{7}$$

K_D was calculated from the measured value of K_M using the measured values of k_e and values of k_{on} estimated by extrapolation of k_2 in Figure 6. (See Appendix.) One difference between the K_D obtained from biphasic kinetics above and the K_D obtained by this procedure is that the former refers to equilibration in the dark state (DQ), whereas this method refers to equilibration in the light state (D^+Q^-). In this work, we ignore the difference between these two states since the difference in K_D is expected to be small (less than a factor of 3 as discussed below).

RESULTS

Binding. The binding constant and second-order rate constants for electron transfer of cyt to native and mutant RCs were measured by monitoring the oxidation and re-reduction of the $Bchl_2$ at a wavelength of 865 nm (Figure 2). A sharp absorption decrease corresponding to the oxidation of $BChl_2$ ($D \rightarrow D^+$), occurred after a laser flash, followed by a recovery ($D^+ \rightarrow D$). In the absence of cyt, the recovery was slow and not observable on the millisecond time scale. In the presence of cyt, the recovery kinetics for most samples show two phases corresponding to the two electron-transfer processes shown in eq 1. A fast phase (not resolved in Figure 2) due to electron transfer from bound cyt occurred with rate constant, k_e. A slow phase, due to reaction of unbound cyt, occurred with a rate that is dependent on cyt concentration and governed by a second-order rate constant k_2. The changes in K_D for different RCs are illustrated in Figure 2 as changes in the fraction of fast phase. Mutation of Leu M191 to Ala results in a smaller amount of fast phase (larger K_D), while mutation of Val M192 to Ala resulted in a larger amount of fast phase (smaller K_D). The values for K_D were determined by

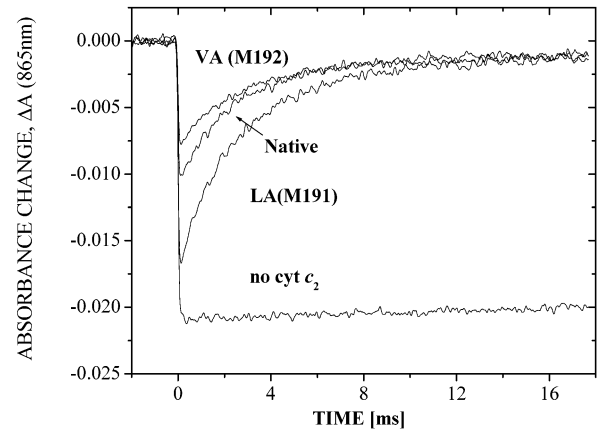

FIGURE 2: Biphasic flash-induced absorbance changes at 865 nm due to $BChl_2$ oxidation and re-reduction in native and mutant RCs VA (M192) [Val M192 → Ala] and LA (M191) [Leu M191 → Ala]. In the absence of cyt, the band at 865 nm recovers slowly (τ > 100 ms). In the presence of cyt, biphasic recovery kinetics were observed. The fast phase (microsecond time scale), unresolved in these traces, is due to reaction of bound cyt. The slow phase is due to second-order reaction of unbound cyt. The free cyt concentrations were the same for all samples containing cyt. The different amounts of fast and slow phases observed for different mutant RCs indicate changes in cyt binding due to mutation ([RC] = 0.23 μM, [cyt c_2] = 0.41 μM, pH 7.5, 10 mM Hepes).

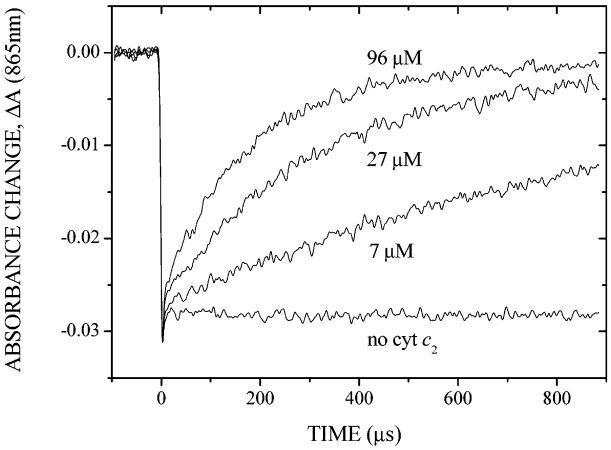

FIGURE 3: Monophasic flash-induced absorbance changes at 865 nm in YA (L162) [Tyr L162 → Ala] RCs. The absorbance change at 865 nm exhibits single-exponential decay with observed rate constants that increase with increasing cyt concentration up to a maximum. This kinetic behavior is attributed to fast exchange of the cyt bound to the RC prior to electron transfer.

measuring the fraction of fast phase as a function of free cyt concentration.

The reaction kinetics for several mutant RCs showed monoexponential kinetic behavior at all cyt concentrations. An example of this is the kinetics for the Tyr L162 → Ala mutant shown in in Figure 3. For these cases, the measured exponential rate constant increased to a saturating value at high cyt concentration. The values for K_D were obtained from eqs 6 and 7. Other examples of this behavior were Tyr L162 → Ser, Leu M191 → Cys, and Leu M191 → Lys. The values of K_D and the free energy changes, $\delta\Delta G$, due to all mutations are shown in Table 1. A comparison of the effects of mutating different residues to Ala or Ser shows that the increase in free energy for binding is greatest for mutation of Tyr L162 and decreases in the order: Tyr L162 > Leu M191> Val M192. This suggests a major role for Tyr L162 in the binding process.

Table 1: Parameters of the Reaction between Native and Mutant RCs and cyt c_2 from *Rb. sphaeroides* (pH 7.5 10 mM Hepes)[a]

RC strain	K_D (μM)	$\delta\Delta G_o$ (meV)	τ_e (μs)	k_2 (10^8 M^{-1} s^{-1})
native RC	0.30	0	0.97	14
LA (M191)	3.0	58	8.8	9
LS (M191)	3.0	58	16.2	10
LH (M191)	4.0	65	1.0 (0.4), 4.5 (0.6)[b]	9
LD (M191)	1.4	39	1.0 (0.4), 5.6 (0.6)[b]	7
LC (M191)	15[c]	111	57	8
LK (M191)	380[c]	180	212	0.12
VS (M192)	0.13	−21	0.55	12
VA (M192)	0.17	−14	0.62	13
VD (M192)	0.5	13	1.0 (0.4), 3.5 (0.6)[b]	14
LA(M191)/ VA (M192)	2.8	56	4.0	8
YF (L162)	4.3	68	4.0	8.3
YL (L162)	8.8	87	42	7.0
YA (L162)	30[c]	125	120	2.0
YS (L162)	30[c]	125	160	1.5

[a] The errors are standard deviations obtained from repeated measurements. For K_D, t_e, and k_2 their values were less than 15% for most samples. Larger errors (~25%) were obtained for measurements of K_D and k_2 for VS(M192) and VA(M192), VD(M192) and for estimation of K_D for LC(M191). [b] Double exponential first-order kinetics observed in these samples at saturating cyt concentrations. The number in parentheses is the fractional amplitude. [c] Single-exponential kinetics observed in these samples under all conditions, indicating fast exchange of the cyt.

Hydrophobic residues were also mutated to other residues (Table 1). The largest change in K_D was due to the mutation Leu M191 → Lys, probably due to the positive charge. A large change in K_D was observed for the Leu M191 → Cys mutation. (Table 1). To determine the nature of the Cys residue, the LC(M191) RCs were treated with *N*-ethyl maleimide (200 μM, 20 h, pH 7.5). No change in either K_D or k_2 was observed. This suggests that the Cys is either inaccessible or has been chemically modified. The nature of the modification is not known.

Results from these studies differ from those of other workers. We do not observe the slow first-order phase reported to be associated with RCs in a distal configuration (*12*). In addition, in the Tyr L162 mutants a larger fraction of fast phase electron transfer for the Phe and Leu mutants was observed and the second-order rate constants were found to be different from previous results (*27*). One possibility for these differences is a aggregation of the RCs as reported by Tiede and co-workers (*34*) that may change the accessibility of the cyt binding site. This aggregation was found to be dependent on RC preparation and may be present at higher protein concentrations used in previous studies.

First-Order Electron Transfer. The first-order electron-transfer rate constant, k_e, for native and mutant RCs were measured on a faster time scale under conditions of high cyt concentrations where the RC is fully bound to cyt (see Figure 4). Both increases and decreases in k_e were found due to mutation of hydrophobic residues. These changes in k_e were correlated with changes in the dissociation constant K_D. LA(M191) RCs showed a ~10-fold decrease in both binding affinity and electron-transfer rate, while VA(M192) RC showed a ~2-fold increase in both binding affinity and electron-transfer rate (Figures 2 and 4, and Table 1).

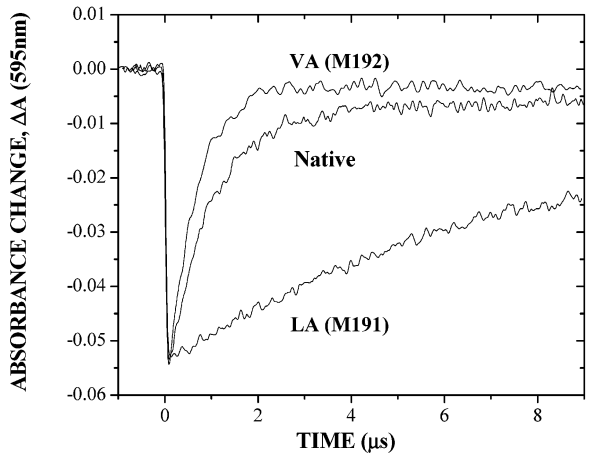

FIGURE 4: Fast phase of electron transfer (microsecond time scale) monitored at 595 nm at saturating cyt concentration due to cyt bound to the RC. The rate constant k_e is independent of cyt concentration. The differences in the decay rates indicate changes in electron-transfer rates of the bound cyt due to mutation. ([RC] = 5 μM, [cyt] = 50 μM, pH 7.5, 10 mM Hepes).

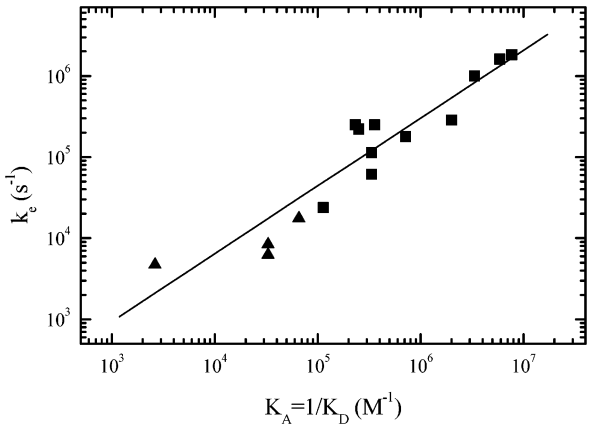

FIGURE 5: Plot of first-order electron-transfer rate k_e vs association constant K_A (log scale). The solid line represents a linear fit with slope, $\gamma = 0.85 \pm 0.1$, and correlation coefficient $R = 0.95$. This shows that the electron transfer and binding changes due to mutation of hydrophobic groups are strongly correlated. The triangles represent samples showing monophasic kinetics.

RCs displaying monophasic kinetics also showed a similar correlation between binding affinity and maximum electron-transfer rate. YA(L162) RCs (Figure 3) showed a ~100 fold decreased binding affinity and maximum electron-transfer rate (Table 1). The results for all mutants are shown in Table 1. In some cases, LD(M191), LH(M191), VD(M192), the first-order rate constants were biphasic. Since these residues are all acidic, the pH dependence of the rate constants was measured. The rate constants were found to be independent of pH over the range from pH 5−9. The biphasic kinetics suggests that two different binding sites for the cyt on the RC surface are occupied. The component with the native rate (10^6 s^{-1}) is likely due to cyt in the native site and the other slower component may be due to cyt displaced to a larger distance.

A general feature of the effects of mutating hydrophobic residues is the correlation between the electron-transfer rate k_e and the association constant, $K_A = 1/K_D$ (Figure 5).

For simplicity, in this plot only the smaller values of k_e for the biphasic kinetics are plotted. The slope, γ, of the log−log plot of k_e vs K_A is $\gamma = 0.85 \pm 0.1$ and the correlation coefficient is $R = 0.95$. The correlation is consistent with a power-law relationship

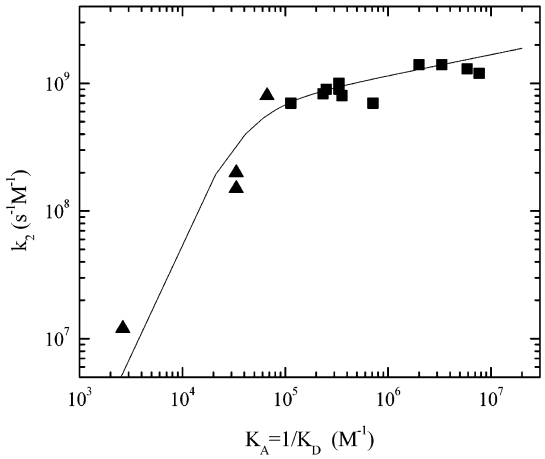

FIGURE 6: Plot of second-order electron-transfer rate k_2 vs association constant, K_A (log scale). The rates fall into two regions, a diffusion controlled ($k_e \gg k_{off}$) region at high K_A, with a small slope, $\alpha = 0.15$, and a fast exchange region ($k_e \ll k_{off}$) at low K_A with a larger slope = 1.7. The RCs displaying monophasic kinetics (triangles) are in the fast exchange region. The solid line represents a fit to the experimental data using a model based on the dependence of k_e and k_{on} on K_A (see Appendix).

$$k_e = CK_A^{\gamma} \tag{8}$$

where C is a constant. These results indicate that the interactions modified by mutation of hydrophobic residues produce similar magnitude of changes of both electron-transfer rate and binding affinity.

Second-Order Electron Transfer. The second-order rate constants, k_2, were determined by measuring the dependence of the rate of the slow kinetic phase (Figures 2 and 3) on the concentration of free cyt (eq 6). The values determined for all samples are shown in Table 1. The value of k_2 (1.4×10^9 s^{-1} M^{-1}) for native RCs was ~20% lower than found in a previous study (*14*) possibly due to the lower cyt concentrations used in this study. The changes in the second-order rate constant due to mutation of hydrophobic residues were relatively small for mutants with small changes in K_D. However, large changes in k_2 were observed for RCs exhibiting large changes in K_A. A log−log plot of the second-order rate constant, k_2, vs binding affinity, K_A, for the modified RCs is shown in Figure 6.

The plot shows two regions, a high affinity region and a low affinity region. These two regions represent two different kinetic regimes for values of the rate constants k_e, k_{on}, and k_{off} shown in eq 1. The experimental results can be fitted (solid line in Figure 6) by a model based on transition state theory and the power law dependence of k_e. (See Appendix.) In the high affinity region, the reaction is diffusion controlled ($k_2 = k_{on}$ from eq 12 where $k_e \gg k_{off}$). The low value of the slope in this region ($\alpha = 0.15 \pm 0.1$) reflects the weak dependence of the association rate k_{on} on the binding energy. In the low affinity region, the reaction is in a fast exchange regime ($k_2 = k_e K_A$ from eq 12 where $k_e \ll k_{off}$). The high slope in this region results from the dependence of the second-order rate on the both k_e and K_A. Additional support for this model is the fact that the samples displaying

monophasic kinetics (triangles in Figure 6) were all in the fast exchange region.

Effect of the Difference in K_D for Light and Dark States. In the treatment of the binding constants and association and dissociation rates discussed above we have neglected the difference between the values obtained for the dark state (DQ) and light state (D^+Q^-). This difference is expected to result from the additional positive charge on D^+ which interacts with positive charges on the cyt surface leading to an association constant for the light state smaller than for the dark state. A limit for this difference comes from the measurements of Larson and Wraight (*16*) who found K_A to be 3-fold larger for oxidized (Fe^{3+}) horse cyt compared to reduced (Fe^{2+}) cyt due to interactions between charges on the Fe and negative surface charges on the RC. Any change in K_A due to the oxidation of $D \rightarrow D^+$ is expected to be less since D^+ is farther from the charges on the cyt surface than the Fe is from the charges on the RC surface (e.g., see Figure 1) and since cyt c_2 is almost neutral (i.e., the interaction between D^+ and cyt is a charge-dipole interaction). We estimate K_A (dark) = 1−3 times K_A (light). Since the quantitative difference has not been measured, no correction has been made. But we note that any difference would result in a slight shift of K_A to larger values for data points for the mutant RCs displaying monophasic kinetics which are indicated by triangles in Figures 5 and 6.

DISCUSSION

In this study, changes in cyt/RC interactions due to single RC mutations replacing the hydrophobic interfacial residues Tyr L162, Leu M191, and Val M192 were examined. The effects of these changes on the binding affinity, K_A, interprotein electron-transfer rate, k_e, and second-order electron-transfer rate constant, k_2, are discussed below.

Binding. Site-directed mutations of interfacial residues have been used extensively to study the role of specific residues in protein association. Systematic mutation of surface residues to Ala (alanine scanning mutagenesis) have revealed some general features. One common feature of interacting proteins is the presence of a central "hot-spot" in the binding interface typically consisting of an aromatic amino acid whose mutation greatly decreases the binding affinity. Surrounding this site is a ring of amino acids whose mutation produces smaller changes (*35*). A correlation was found between the free energy change upon mutation and the fraction of solvent accessibility of the residue in the complex (*35*).

The results of the present study show some of these characteristic features. The effect of replacing Tyr L162 by Ala is larger than that of replacing Leu M191 or Val M192. The values of K_D are changed by factors of 100, 10, and 0.5, respectively. This indicates that Tyr L162 is a "hot-spot" on the binding surface. The small effect of mutating Val M192 correlates with its larger distance from the hot spot and can be related to solvent accessibility. This is shown schematically in Figure 7 by a map of the free energy changes for mutation to Ala on RC surface residues colored according to their solvent accessibility.

The short-range interaction region generally is in the region shown in dark blue (low solvent accessibility) in the center of the RC surface. Tyr L162 and Leu M191 both display large free energy changes upon mutation and low solvent accessibility (2 and 0.5%, respectively). However, Val M192 is at the periphery close packed surface and displays a small negative free energy change upon mutation and a high solvent accessibility (35%). This high solvent accessibility can explain the small effect of its mutation on the binding affinity.

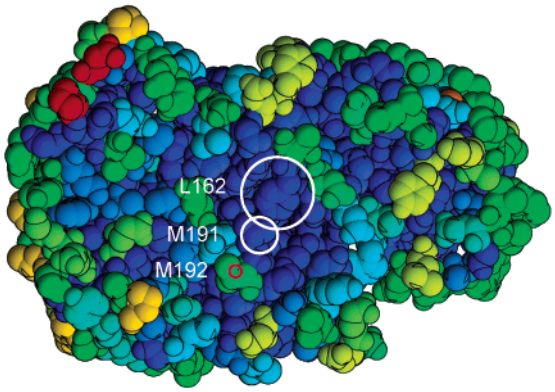

FIGURE 7: Changes in binding free energy, $\delta\Delta G$, due to mutation of hydrophobic residues mapped on RC surface residues colored according to their solvent accessibility. The diameters of the circles are proportional to $\delta\Delta G$ (white positive, red negative). The residues are colored using a scale related to their fractional solvent accessibility in the cyt/RC complex, lowest accessibility (dark blue) and highest accessibility (red). The short-range interactions occur in the region of low solvent accessibility (close packing) surrounding the "hot spot", Tyr L162. The percent solvent accessibility of the mutated residues are 2, 0.5, and 35 for Tyr L162, Leu M191, and Val M192, respectively. The small $\delta\Delta G$ due to mutation of Val M192 may be due to its high solvent accessibility. The solvent accessibility was determined using the Lee-Richards algorithm (*36*) using the CNS program (*37*) with a rolling ball of radius 1.4 Å.

The changes in free energy upon mutation have been explained by creation of defects (voids or conformational changes) in the closely packed residues in the protein−protein interface that reduce the binding energy (*38*). Thus, the decreased binding affinity due to mutation of Tyr L162 and Leu M191 could be due to the loss of van der Waals contacts resulting from mismatch between the surfaces in the modified complex. The small effect of mutating Val M192 may be due to the filling of defects at the interface by water molecules. Since the Val M192 is surface accessible, the solvation could occur breaking hydrogen bonds between water molecules and thus without a large energy penalty. It has been noted that the changes in binding energy upon mutation are perturbations to the binding energy and are not equal to the hydrophobic contributions to the binding energy (*38*). Thus, though mutation of Val M192 to Ala does not greatly decrease the binding energy, interactions of Val M192 at the interface may still contribute to the binding energy between cyt and RC. The interactions of Val M192 with the cyt (e.g., Figure 1) lost upon mutation could be compensated by interactions with water molecules.

First-Order Electron Transfer. The first-order electron-transfer rate, k_e, is the interprotein electron-transfer rate from a cyt bound in the cyt/RC complex. Previous studies showed that mutations of charged residues in the region surrounding the central short-range interaction domain did not result in changes in the first-order electron-transfer rate, k_e (*14*). This was interpreted as indicating that the long-range interactions in the well-solvated electrostatic domain did not determine

the tunneling matrix element at the binding interface. The interactions important for interprotein electron transfer were attributed to short-range van der Waals interactions in the center of the binding region. In the present work, large changes in first-order electron-transfer rates were observed due to mutation of hydrophobic residues in the short-range interaction region (Figure 5). This result supports the proposal that the short-range hydrophobic interactions play an important role in orienting the cofactors at the tunneling interface between the two proteins.

An interesting result of the present study is the observation that the first-order interprotein electron-transfer rate, k_e, is strongly correlated with the binding affinity K_A (Figure 5). The correlation between k_e and K_A can be explained by considering the theory of electron transfer in the bound state (*4*, *39*). The rate of electron transfer can be described as the product of the square of a tunneling matrix element and a Franck−Condon factor. The classical form of the Franck−Condon factor is the Marcus relation which describes the free energy dependence of k_e in terms of the change in electron free energy, ΔG_e, due to electron transfer and a reorganization energy, λ (*4*). Although mutation of hydrophobic residues could change ΔG_e or λ, these changes are not likely to be large since the electron-transfer cofactors are in the interior of the protein and out of contact with the binding interface. For instance, the binding of horse cyt *c* to RC changes the redox potential of the cyt by 29 meV (*16*) compared to the value of the cyt in solution. The charge reversing mutation of a surface Asp M184 group to Lys on the RC changed the redox potential of D^+/D by 14 meV (*14*). The mutations of hydrophobic residues are likely to result in even smaller changes to the redox potentials (and also λ) than these, since for the most part, changes in charges that can effect redox potentials through long-range electrostatic interactions are not involved. Thus, the observed changes in rate, of up to 100-fold, are not expected to result from changes in the Franck−Condon factor.

The most likely explanation for the change in rate is a change in the tunneling matrix element. The exponential decay of the matrix element with distance leads to an exponential dependence of the electron-transfer rate with distance (*40*).

$$k_e = k_o e^{-\beta r} \tag{9}$$

where k_o and β are constants. An increase in the distance between contact surfaces in the short-range tunneling interface region would decrease the rate due to a lower tunneling interaction. It would also weaken the van der Waals contacts at the tunneling interface leading to a decrease in the binding affinity. Assuming the change in k_e is due to a change in the electron-tunneling matrix element, estimation of the change in distance produced by the mutation can be obtained using the exponential dependence of rate on distance, eq 8. Continuum models for electron transfer through a homogeneous medium have used different values of the distance decay parameter $\beta = 1.1-1.4$ Å^{-1} (*40*, *41*) leading to changes in distance between cofactors of 3.3−4.2 Å for a 100-fold change in k_e. The pathway model for electron transfer describes electron transfer through specific bonded or nonbonded (through-space) contacts (*42*). For electron transfer from cyt to RC, a large decrease in the matrix element comes from the through-space jump between the exposed heme edge and Tyr L162 on the RC (*43*). This contact is likely to be modulated by mutations of Tyr L162 as well as other hydrophobic interfacial residues. The distance decay parameter for static through-space decay is large, $\beta = 3.4$ Å^{-1}. Thus, a 1.3 Å change in distance could produce a 100-fold change in rate. In addition, it has been proposed that fluctuations in the nonbonded distance could lead to transient tunneling contacts and faster rates (*44*). Thus, several different models could be used to explain the changes in k_e due to changes in tunneling distance due to mutation of hydrophobic residues. If the change in rate is due to an exponential change in distance, the correlation shown in Figure 5 implies that the binding free energy changes linearly with the change in tunneling distance. While the distance dependence can explain the correlation between k_e and K_A, it does not explain the molecular basis for the rather surprising quantitative correlation between the two quantities. More studies are necessary to clarify this question.

Alternative explanations for the correlation between k_e and K_A are suggested by the observation that the two quantities are almost proportional (γ close to 1.0). This could be explained by models that involve equilibration or transitions between different states (instead of electron transfer from a single state discussed above). While such alternative models would be very appealing, several simple two-state models, discussed below, do not appear to explain the experimental observations. (i) The dependence of k_e on binding affinity could be explained if the electron-transfer rate is proportional to the occupancy of the bound state relative to the unbound state. However, since the first-order electron-transfer rate, k_e, is measured at saturating cyt concentration (i.e., is independent of cyt concentration), the bound state is fully occupied. (ii) A correlation between k_e and K_A could result from rapid equilibration between two *bound* states, one active in electron transfer and another inactive, if decreased binding affinity reduced the occupancy of the active state (i.e., if the mutations only affect the energy of the active state). However, changes in binding and rate would only be observed if both states had appreciable occupancy, thus the model would not give a proportionality over such a wide range (1000-fold) of binding affinity. (iii) A correlation between k_e and K_A could result from a slow reaction between two bound states if k_e is limited by conformational gating across a transition state barrier whose height depends on the binding energy (Brönsted coeffient $\alpha \sim 1.0$). However, k_e is dependent upon driving force as expected for a typical electron-transfer reaction (*45*, *46*) and therefore is not limited by a gating process. While these simple models are inadequate to explain the experimental results, perhaps more complex models involving conformational equilibria or dynamics could provide an explanation.

Second-Order Electron Transfer. The second-order rate constant, k_2, depends on the microscopic rate constants k_{on}, k_{off}, and k_e in eq 1. Depending on the values of these rate constants the reaction mechanism can fall in one of two regimes, the diffusion limit for $k_e \gg k_{off}$, or the fast exchange limit for $k_{off} \gg k_e$. The effects of hydrophobic mutations on k_2 is different in the two regimes (see Figure 6 and Appendix).

For the native cyt and RC as well as mutants that display high binding affinity, the second-order rate constant k_2 is in

the diffusion limit ($k_e \gg k_{off}$). In this limit, k_2 is determined by the rate of protein association that leads to the cyt/RC complex oriented in a proper configuration for electron transfer, $k_2 = k_{on}$. This is supported by experiments that show k_2 to be independent of driving force for electron transfer (*45*). Previous studies showed that mutations of charged residues produce significant changes in k_2 that were correlated with changes in the association constant K_A (*14*). The Brönsted coefficient, α, the slope of the log−log plot of k_2 vs K_A, was relatively large ($\alpha \approx 0.4$). A large value for α indicates a similarity between the structure of the cyt/RC complex in the transition state with that of the cyt/RC complex in the final bound state in which the cofactors are in juxtaposition for electron transfer. The value of $\alpha = 0.4$ due to mutation of charged residues can be explained by the long-range nature of electrostatic interactions. Electrostatic calculations of the effects of charged mutations on k_2 suggest a transition state in which the cyt is ~10 Å from the surface of the RC (*6*).

In the present study, the changes in second-order rate constants due to mutations of hydrophobic residues were relatively small compared to the changes in the binding constant, K_A, for the high affinity region in the log−log plot of k_2 vs K_A (Figure 6). The low value of the slope (Brönsted coefficient) in this region, $\alpha = 0.15$, shows that mutations of hydrophobic residues do not greatly change the energy of the transition state (*47*). This is consistent with the proposed large distance between the cyt and RC at the transition state. The short-range interactions between hydrophobic residues on the cyt and the mutated hydrophobic residues on the RC come into effect only after the transition state is formed, i.e., when the complex is well on its way to the final configuration active in electron transfer. The effects of short-range contacts are to reduce the dissociation rate k_{off} of the cyt but do not greatly change the association rate k_{on}.

While the effect of mutation of hydrophobic residues on k_2 is small in the diffusion limiting case, the effect of these mutations on k_2 can be large if the reaction is in the fast exchange regime (see Figure 6). The second-order rate constant in the fast exchange regime is slow because the cyt dissociates before electron transfer is accomplished ($k_e < k_{off}$). Thus, the cyt/RC complex forms and dissociates many times before the electron-transfer reaction occurs. In this regime, $k_2 = k_e K_A$ (Appendix). Thus, k_2 is reduced by the changes in both k_e and K_A. The second-order rate constant is greatly reduced by hydrophobic mutations in this regime because the fraction of cyt bound is smaller and the electron-transfer rate from the bound cyt is slower. The change in k_e as well as K_A explains why mutations to residues in the hydrophobic domain but not in the electrostatic domain (*14*) produce second-order rates in the fast exchange limit (i.e., monophasic kinetics). Since mutations to charged residues do not appreciably change k_e, larger decreases in k_{off} would be required to reach the fast exchange condition compared to mutation of hydrophobic residues.

Mechanism for Binding and Electron Transfer. The role of charged and hydrophobic residues in the electron-transfer mechanism can be summarized as follows. Long-range electrostatic interactions bring the reactive surfaces the cyt and RC together in an encounter complex. Movement of the cyt within the encounter complex results in the orientation of the two surfaces into a transition state similar to that of the bound state. The distance between the cyt and RC in the transition state is ~10 Å. The final step in the binding is the desolvation of the interface, forming short range van der Waals and hydrogen-bond contacts, fixing the two tunneling surfaces in close proximity, thereby facilitating electron transfer. The present study supports this model and points to an important role of the hydrophobic residues, particularly Tyr L162 in both binding and electron transfer. A surprising result from this study was the finding that the changes in binding and electron transfer rate were strongly correlated. Further studies of these effects including mutation of the complementary Phe C102 residue on cyt c_2 are in progress and should help to provide more detailed information about the molecular basis for binding and electron transfer.

ACKNOWLEDGMENT

We thank Dieter Oesterhelt and Joe Farchaus for providing us with *Rb. sphaeroides* mutant strains with Tyr L162 replaced by Phe, Leu, and Ser, Herb Axelrod for solvent accessibility calculations, Charlene Chang for construction of site-directed mutants, and George Feher, Osamu Miyashita, and Jose Onuchic for discussions of binding and electron transfer.

APPENDIX: RELATION BETWEEN k_2 AND K_A

The second-order rate constant, k_2, is defined in terms of the reaction scheme shown in eq 1. Before the flash the bound and unbound states are in equilibrium where the association constant K_A is

$$K_A = \frac{1}{K_D} = \frac{k_{on}}{k_{off}} \tag{10}$$

After the flash, the slow rate of electron transfer due to reaction of unbound cyt is given by a second-order rate process

$$\text{rate} = k_2[\text{cyt}][D^+Q^-] = k_{obs}[D^+Q^-] \tag{11}$$

In this work, we have ignored the difference in K_D for cyt binding to the RC before and after the flash (see footnote 2).The value of k_2 is related to the values of the rate constants k_{on}, k_{off}, and k_e from eqs 6 and 7 at low cyt concentration, $[\text{cyt}] \ll K_M$ (*47*)

$$k_2 = \frac{k_{on}k_e}{k_{off} + k_e} \tag{12}$$

The relation between k_2 and K_A is derived below. The values of k_e for different mutant RCs vary with K_A as shown experimentally in Figure 5

$$k_e = k_e^o\left(\frac{K_A}{K_A^o}\right)^\gamma \tag{13}$$

k_e^o and K_A^o are the values for the native RCs and k_e and K_A are the parameter values for mutant RCs. The values for the association rate, k_{on}, are expected to have a similar dependence on K_A, i.e., the log−log plot (Brönsted plot) of k_{on} vs K_A is expected to be linear (*14*). The Brönsted coefficient α

is the ratio between the change in the free energies of transition state $\delta\Delta G_o^{\ddagger}$ and the change in free energy of the bound state $\delta\Delta G_o$ due to mutation, $\delta\Delta G_o^{\ddagger} = \alpha\delta\Delta G_o$. The value of α is assumed the same for all hydrophobic mutants.

$$k_{on} = k_{on}^{o}\left(\frac{K_A}{K_A^{o}}\right)^{\alpha} \tag{14}$$

The parameters γ and α refer to different processes (intermolecular electron transfer and protein association) and are expected to have different origins. The origin of the parameter γ is not known. Substituting the expressions for k_{on} and k_e into eq 12 yields a relation between k_2 and K_A

$$k_2 = \frac{k_e^{o}\left(\frac{K_A}{K_A^{o}}\right)^{\gamma}}{\frac{k_e^{o}}{k_{on}^{o}}\left(\frac{K_A}{K_A^{o}}\right)^{\gamma-\alpha} + K_A^{-1}} \tag{15}$$

This relation gives a good fit to the data in Figure 6 using the known values for $k_{on}^{o} = 1.4 \times 10^9\ s^{-1}\ M^{-1}$, $k_e^{o} = 1.0 \times 10^6\ s^{-1}$, $K_A^{o} = 3.3 \times 10^6\ M^{-1}$ and $\gamma = 0.85$. The only adjustable parameter was the value for $\alpha = 0.15 \pm 0.05$. Two regimes of electron-transfer result from this model: the diffusion-limited regime ($k_e \gg k_{off}$) and the fast exchange regime ($k_e \ll k_{off}$). The crossover between these two regimes occurs when $k_e = k_{off}$ at a value of $K_A = 3.3 \times 10^4\ M^{-1}$ ($K_D = 30 \times 10^{-6}$ M).

REFERENCES

1. Cramer, W. A., and Knaff, D. B. (1990) *Energy Transduction in Biological Membranes*, Springer-Verlag, New York.
2. Bendall, D. (1996) in *Protein Electron Transfer* (Bendall, D., Ed.) pp 43−68, Bios Scientific Publishers Ltd, Oxford, UK.
3. Mathews, F., Mauk, A., and Moore, G. (2000) in *Protein−Protein Recognition* (Kleanthous, C., Ed.) pp 60−101, Oxford, UK.
4. Marcus, R. A., and Sutin, N. (1985) *Biochim. Biophys. Acta 811*, 265−322.
5. Northrup, S. H. (1996) in *Protein Electron Transfer* (Bendall, D., Ed.) pp 69−94, Bios Scientific Publishers, Oxford, UK.
6. Miyashita, O., Onuchic, J. N., and Okamura, M. Y. (2003) *Biochemistry*, in press.
7. Axelrod, H. L., Abresch, E. C., Okamura, M. Y., Yeh, A. P., Rees, D. C., and Feher, G. (2002) *J. Mol. Biol. 319*, 501−515.
8. Feher, G., Allen, J. P., Okamura, M. Y., and Rees, D. C. (1989) *Nature (London) 339*, 111−116.
9. Dutton, P. L., and Prince, R. C. (1978) in *The Photosynthetic Bacteria* (R. C. Clayton, W. R. S., Ed.) pp 525−570, Plenum Press, New York.
10. Prince, R. C., Cogdell, R. J., and Crofts, A. R. (1974) *Biochim. Biophys. Acta 347*, 1−13.
11. Dutton, P. L., Petty, K. M., Bonner, H. S., and Morse, S. D. (1975) *Biochim. Biophys. Acta 389*, 536−556.
12. Moser, C., and Dutton, P. L. (1988) *Biochemistry 27*, 2450−2461.
13. Overfield, R. E., Wraight, C. A., and Devault, D. C. (1979) *FEBS Lett. 105*, 137−142.
14. Tetreault, M., Rongey, S. H., Feher, G., and Okamura, M. (2001) *Biochemistry 40*, 8452−8462.
15. Tiede, D., and Dutton, P. (1993) in *The Photosynthetic Reaction Center* (Deisenhofer, J., and Norris, J., Eds.) pp 258−288, Academic Press, San Diego.
16. Larson, J., and Wraight, C. (2000) *Biochemistry 39*, 14822−14830.
17. Gerencser, L., Laczko, G., and Maroti, P. (1999) *Biochemistry 38*, 16866−16875.
18. Hall, J., Zha, X., Durham, B., O'Brien, P., Vieira, B., Davis, D., Okamura, M., and Millett, F. (1987) *Biochemistry 26*, 4494−4500.
19. Rosen, D., Okamura, M. Y., Abresch, E. C., Valkirs, G. E., and Feher, G. (1983) *Biochemistry 22*, 335.
20. Caffrey, M. S., Bartsch, R. G., and Cusanovich, M. A. (1992) *J. Biol. Chem. 267*, 6317−6321.
21. Tetreault, M., Cusanovich, M., Meyer, T., Axelrod, H., and Okamura, M. (2002) *Biochemistry 41*, 5807−15.
22. Allen, J. P., Feher, G., Yeates, T. O., Rees, D. C., Deisenhofer, J., Michel, H., and Huber, R. (1986) *Proc. Natl. Acad. Sci. U.S.A. 83*, 8589−8593.
23. Tiede, D. M., and Chang, C.-H. (1988) *Isr. J. Chem. 28*, 183−191.
24. Adir, N., Axelrod, H., Beroza, P., Isaacson, R., Rongey, S., Okamura, M., and Feher, G. (1996) *Biochemistry 35*, 2535−2547.
25. Tiede, D., Vashishta, A., and Gunner, M. (1993) *Biochemistry 32*, 4515−4531.
26. Farchaus, J., Wachtveitl, J., Mathis, P., and Oesterhelt, D. (1993) *Biochemistry 32*, 10885−10893.
27. Wachtveitl, J., Farchaus, J., Mathis, P., and Oesterhelt, D. (1993) *Biochemistry 32*, 10894−10904.
28. Dohse, B., Mathis, P., Wachtveitl, J., Laussermair, E., Iwata, S., Michel, H., and Oesterhelt, D. (1995) *Biochemistry 34*, 11335−11343.
29. Gong, X.-M., Paddock, M., Chang, C., Feher, G., and Okamura, M. (2003)*Biophys. J. Suppl. 84*, 150a.
30. Paddock, M. L., Adelroth, P., Chang, C., Abresch, E. C., Feher, G., and Okamura, M. Y. (2001) *Biochemistry 40*, 6893−6902.
31. Tetreault, M., Cusanovich, M., Meyer, T., Feher, G., and Okamura, M. Y. (1999) *Biophys. J. 76*, A20.
32. Bartsch, R. (1978) in *The Photosynthetic Bacteria* (Clayton, R., and Sistrom, W., Eds.) pp 249−279, Plenum Press, New York.
33. Brandner, J. P., McEwan, A. G., Kaplan, S., and Donohue, T. J. (1990) *J. Bacteriology 171*, 360−368.
34. Tiede, D. M., Littrell, K., Marone, P. A., Zhang, R., and Thiyagarajan, P. (2000) *J. Appl. Crystallogr. 33*, 560−564.
35. Bogan, A., and Thorn, K. (1998) *J. Mol. Biol. 280*, 1−9.
36. Lee, B., and Richards, F. M. (1971) *J. Mol. Biol. 55*, 379−400.
37. Brünger, A. T., Adams, P. D., Clore, G. M., DeLanod, W. L., Gros, P., Grosse-Kunstleve, R. W., Jiangf, J.-S., Kuszewski, J., Nilges, M., Pannu, N. S., Read, R. J., Rice, L. M., Simonson, T., and Warren, G. L. (1998) *Acta Crystallogr. D54*, 905−921.
38. DeLano, W. (2002) *Curr. Opin. Struct. Biol. 12*, 14−20.
39. Hopfield, J. J. (1974) *Proc. Natl. Acad. Sci. U.S.A. 71*, 3640.
40. Moser, C. C., Keske, J. M., Warnke, K., Farid, R. S., and Dutton, P. L. (1992) *Nature 355*, 796−802.
41. Tezcan, F., BR, C., Winkler, J., and Gray, H. (2001) *Proc. Natl. Acad. Sci. U.S.A. 98*, 5002−5006.
42. Onuchic, J. N., Beratan, D. N., Winkler, J. R., and Gray, H. B. (1992) *Annu. Rev. Biophys. Biomol. Struct. 21*, 349−77.
43. Aquino, A., Beroza, P., Beretan, D., and Onuchic, J. (1995) *Chem. Phys. 197*, 277−288.
44. Aquino, A., Beroza, P., Reagan, J., and Onuchic, J. (1997) *Chem. Phys. Lett. 275*, 181−187.
45. Lin, X., Williams, J. C., Allen, J., and Mathis, P. (1994) *Biochemistry 33*, 13517−13523.
46. Venturoli, G., Drepper, F., Williams, J., Allen, J., Lin, X., and Mathis, P. (1998) *Biophys. J. 74*, 3226−3240.
47. Fersht, A. (1999) *Structure and Mechanism in Protein Science*, W. H. Freeman and Co., New York.

BI035603C